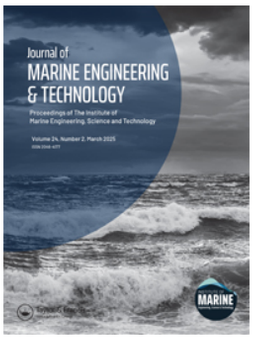

Journal of Marine Engineering & Technology

ISSN: (Print) (Online) Journal homepage: www.tandfonline.com/journals/tmar20

Methanol sprays in marine engines: CFD modelling of port fuel injection systems

Konstantinos Zoumpourlos, Cemil Bekdemir, Rinze Geertsma, Robert van de Ketterij & Andrea Coraddu

To cite this article: Konstantinos Zoumpourlos, Cemil Bekdemir, Rinze Geertsma, Robert van de Ketterij & Andrea Coraddu (06 Mar 2025): Methanol sprays in marine engines: CFD modelling of port fuel injection systems, Journal of Marine Engineering & Technology, DOI: 10.1080/20464177.2025.2473184

To link to this article: https://doi.org/10.1080/20464177.2025.2473184

Published online: 06 Mar 2025.

JOURNAL OF MARINE ENGINEERING & TECHNOLOGY
https://doi.org/10.1080/20464177.2025.2473184

Taylor & Francis
Taylor & Francis Group

OPEN ACCESS Check for updates

Methanol sprays in marine engines: CFD modelling of port fuel injection systems

Konstantinos Zoumpourlos [a], Cemil Bekdemir[b], Rinze Geertsma [c], Robert van de Ketterij [c] and Andrea Coraddu [a]

[a]Department of Maritime & Transport Technology, Delft University of Technology, Delft, The Netherlands; [b]TNO Powertrains, Helmond, The Netherlands; [c]Faculty of Military Sciences, Netherlands Defence Academy, Den Helder, The Netherlands

ABSTRACT

The maritime sector aims to achieve short and medium-term sustainability targets through the conversion of Internal Combustion Engines to methanol operation. For small to medium sized engines, Port Fuel Injection (PFI) is the most viable injection method to achieve this conversion. However, the knowledge of the behaviour of methanol in combustion engines, particularly its spray characteristics under PFI conditions, is limited. To better understand liquid methanol sprays, this paper studies the injection of methanol in marine PFI conditions through Computational Fluid Dynamics (CFD) modelling. The CFD models use the Lagrangian-Eulerian (LE) coupling method within the Reynolds Averaged Navier Stokes (RANS) turbulence framework. Numerical results were validated using dedicated methanol experiments from the literature for both high and low injection pressures. Subsequently, this predictive CFD framework was used in a number of different injection pressures with scaled injection quantities that represent marine applications. Moreover, we demonstrated that high injection pressure improves atomisation and, thus, evaporation prior to wall impingement. This work strongly contributes to our understanding of marine PFI methanol engines by modelling fuel quantities relevant for ship applications. Our approach can be implemented in full engine simulations to solve evaporation challenges often found in small-bore methanol marine engines.

ARTICLE HISTORY
Received 24 April 2024
Accepted 24 February 2025

KEYWORDS
Methanol; marine internal combustion engines; computational fluid dynamics; spray; port fuel injection

Abbreviations

ICE	Internal combustion engine
CFD	Computational fluid dynamics
PFI	Port fuel injection
DI	Direct injection
CI	Compression ignition
SI	Spark ignition
LE	Lagrangian Eulerian
LPT	Lagrangian particle tracking
RANS	Reynolds averaged Navier Stokes
ECN	Engine combustion network
CVC	Constant volume chamber
HP	High pressure
LP	Low pressure
LHV	Lower heating value
3D	three-dimensional
PISO	Pressure implicit with splitting of operators
CFL	Courant-Friedrichs-Lewy
AMR	Adaptive mesh refinement
We	Weber number
TKE	Turbulent kinetic energy
k_0	Initial turbulent kinetic energy
ε_0	Initial turbulent kinetic energy dissipation rate
ρ_g	ambient air density
ρ_l	liquid density
u_r	relative velocity between the droplet and the gas
r_d	droplet radius
σ	droplet surface tension
KH-RT	Kelvin Helmholtz – Rayleigh Taylor
TAB	Taylor Analogy Breakup
NTC	No time counter
r_c	child droplet radius
r_p	parent droplet radius
Ω_{KH}	growth rate of Kelvin Helmholtz waves
Λ_{KH}	wavelength of fastest growing unstable Kelvin Helmholtz surface wave
τ_{KH}	Kelvin Helmholtz breakup time
B_0	Kelvin Helmholtz model size constant
B_1	Kelvin Helmholtz breakup time constant
Λ_{RT}	wavelength of fastest growing unstable Rayleigh Taylor surface wave
τ_{RT}	Rayleigh Taylor breakup time
Ω_{RT}	growth rate of Rayleigh Taylor waves
C_{RT}	Rayleigh Taylor model size constant
C_τ	Rayleigh Taylor breakup time constant
C_d	Discharge coefficient
P_{inj}	Injection Pressure

1. Introduction

Internal combustion engines (ICEs) are the main source of power and propulsion in the marine sector, which contribute to global warming when using fuels from fossil sources (International Maritime Organization 2020; Kessel 2000; Nemati et al. 2022). Given the ongoing reliance on ICEs (Reitz et al. 2020), to overcome the increasing CO_2 emissions, alternative fuels, such as ammonia and methanol, can promote sustainability in the maritime sector (Ait Allal et al. 2019; Korberg et al. 2021; McKinlay et al. 2021; Curran et al. 2024). Methanol has been identified as an adequate alternative fuel for marine engines due to its scalable production,

CONTACT Konstantinos Zoumpourlos k.zoumpourlos@tudelft.nl Department of Maritime & Transport Technology, Faculty of Mechanical Engineering, Delft University of Technology, Building 34, Mekelweg 2, 2628CD Delft, The Netherlands

promising properties (e.g. liquid state at atmospheric conditions, high laminar flame speed, low combustion temperature etc.), and lower hazardous emissions compared to diesel and gasoline (NO_x, SO_x, and PM) (Soni and Gupta 2016; Verhelst et al. 2019; Zincir and Deniz 2021; Pipicelli et al. 2022). For methanol operation, installing port fuel injection (PFI) systems is the most viable conversion method for current four-stroke medium- and high-speed maritime engines (Verhelst et al. 2019; Dierickx et al. 2021), as space and cost issues limit the adoption of direct injection (DI) systems. However, integrating methanol in marine ICEs involves a high degree of complexity. This complexity is caused by its high latent heat of evaporation, which hinders the mixture formation (Verhelst et al. 2019). Methanol's spray characteristics and mixture formation process are insufficiently studied. For these reasons, evaluating the physical phenomena in PFI methanol sprays is essential.

Previous experimental research on methanol sprays has mainly focussed on atmospheric ambient temperature conditions and relatively low to medium injection pressures (Wang et al. 2005; Gong et al. 2007; Zeng et al. 2010, 2012b; Liu et al. 2022; Wouters et al. 2023). These studies reported similarities between the spray structure of methanol and conventional fuels, indicating only minor differences in the cone angle and spray penetration length. In a study by Zeng et al. (2012a), flash boiling methanol sprays were evaluated at 50 bar injection pressure. The authors stated that the flash boiling phenomenon could improve the start-ability of the engines under cold-start conditions due to enhanced atomisation. In another study by Badawy et al. (2022), lowering the ambient pressure in the flashing regime decreased the droplet sizes, which improved the mixture formation.

More recently, several studies (Matamis et al. 2020; Ghosh and Ravikrishna 2021; Wang et al. 2022) have addressed DI engine conditions under high injection pressures and high ambient temperatures and pressures. In particular, Wang et al. (2022) conducted experiments under compression ignition (CI) conditions and compared methanol with diesel sprays. They reported that at moderate ambient temperatures (600 K), methanol shows improved evaporation due to its lower boiling point. Generally, the reported experiments highlighted many similarities in the macroscopic spray structure between methanol and conventional fuels. Yet, these studies do not quantify the evaporation cooling effect of methanol, and its implications on the air-fuel mixture formation. Therefore, to sufficiently understand methanol sprays, predictive computational fluid dynamics (CFD) models are essential to appropriately characterise spray structure and behaviour under engine conditions. However, the limitations of the current experimental studies make CFD model validation difficult.

To provide CFD model validation, the engine combustion network (ECN), an international collaboration between several institutions, was established, offering an online database of experimental data for conventional fuels (ECN; Maes et al. 2020). Although quite extensive, this database does not cover methanol sprays, especially under PFI conditions. Very limited research has been published regarding CFD studies as experimental data is scarce. Only one study has investigated methanol sprays numerically (Cabezas et al. 2022). In that study, Cabezas et al. (2022) developed a validated gasoline CFD model, which incorporated data from the ECN Spray G (Spray G). The validated spray model was applied on a number of methanol spray conditions representing a spark ignition (SI) DI engine. The authors reported that methanol flash-boiling conditions exhibit an increased evaporation rate, which agrees with previous experimental efforts (Zeng et al. 2012a; Badawy et al. 2022). This shows that CFD simulations can adequately represent underlying spray physics under flash boiling. While the work by Cabezas et al. (2022) improved our understanding of DI methanol engines, a similar CFD approach for PFI methanol engines does not exist indicating a gap in knowledge.

1.1. Aim & novelty

This paper aims to investigate the injection of methanol under marine PFI conditions (i.e. low ambient pressure and temperature, and low injection pressure). The novelty of the present work constitutes of a spray modelling approach, which is validated using methanol experimental data for both high and low injection pressures. This approach can be implemented in the modelling of methanol engine conversion and attain robust operation under PFI operation. For the spray analysis, we used CFD simulations with Lagrangian-Eulerian (LE) coupling methods for the treatment of liquid droplets and the air-fuel gaseous mixture. To validate our models, we benchmarked two methanol injection experiments reminiscent of PFI conditions comprising of a relatively low ambient pressure. These included a high pressure (HP) injection experiment by Ghosh et al. (2020), and a low pressure (LP) injection experiment by Liu et al. (2022).

To achieve an acceptable prediction of liquid penetration, we assessed the choice of various spray parameters (i.e. rate of injection, cone angle, and turbulence model). The assessment demonstrated the influence of these parameters on spray characteristics, such as the liquid length. Moreover, we increased the injection quantity of the validated model to examine the resulting methanol spray characteristics in marine engines. This study provides insights on the impact of injection pressure on droplet breakup, evaporation, and velocity magnitudes. The results indicated that increased injection pressure significantly improves spray atomisation due to enhanced air entrainment.

Coupling the presented modelling framework with 3D engine models can provide a solid modelling methodology to support methanol engine conversion. Our study explains previously reported limitations in increasing methanol energy fraction, and combustion instability of small-bore marine and heavy-duty automotive engines using PFI of methanol. These findings can potentially contribute to methanol implementation in the maritime sector by guiding the CFD modelling of future methanol ICEs.

2. Background

2.1. Methanol in marine engines

Methanol offers desirable physical and chemical properties, which render it suitable for marine engines (Curran et al. 2024). Depending on the engine size, methanol is injected either in the port, through a PFI system, or through a DI system in the cylinder. Based on the piston size, Curran et al. (2024) classified marine engines as small-bore (up to 280 mm), medium-bore (280–500 mm), and large-bore (500–960 mm). Large-bore marine engines typically employ a DI system for methanol injection through a second injector (MAN Energy Solutions) or a co-axial dual fuel injector (Portin 2015). On the other hand, small-bore marine engines, due to space and cost limitations, use a PFI system for methanol premixing and a DI system for diesel pilot ignition (Dierickx et al. 2019, 2021; Agarwal et al. 2022). However, PFI systems are notable for their poor mixture formation because of the low injection pressure, and low ambient pressure and temperature environment in the intake manifold (Zhu et al. 2021; Zoumpourlos et al. 2023). Therefore, retrofitting these engines challenges engine manufacturers and ship owners and delays the implementation of methanol in the maritime sector.

Table 1. Marine fuel properties (American Bureau of Shipping ABS; Agarwal et al. 2019; Verhelst et al. 2019; Kurien and Mittal 2022).

Property	Diesel	Methane	Methanol	Ammonia
Lower Heating Value (LHV) [MJ/kg]	42.7	50	20.1	18.8
Density (at STP) [kg/m^3]	840	0.65	790	0.718
Heat of Vaporization (at 1 bar) [kJ/kg]	250	510	1089	1370
Boiling Point (at 1 bar) [°C]	180–360	−161.5	65	−33.34
Surface Tension (at 20°C) [mN/m]	27	–	23	18.1 (at 34.1°C)
Dynamic Viscosity (at 20°C) [mPa · s]	2.1–2.52	0.01	0.57	0.01

Compared to diesel, methanol has approximately four times higher latent heat of vaporisation (Table 1). This also challenges the creation of a homogeneous mixture by requiring more heat and time for the evaporation of the fuel. Additionally, methanol's lower heating value (LHV) is approximately half of diesel's, thus demanding twice the fuel mass for the same power output (Zincir and Deniz 2021; Pipicelli et al. 2022; Singh et al. 2022). This leads to longer injection duration or larger injector diameter to achieve the same power density as diesel operation. These two properties further complicate methanol retrofitting, often limiting the engine operating range (Panda and Ramesh 2022). We refer to Verhelst et al. (2019) for further information on methanol properties.

For efficient methanol conversion, CFD modelling offers insight into the mixture formation and can potentially identify the best routes to overcome the aforementioned challenges. To model PFI conditions, we distinguish three categories of CFD simulations: spray modelling, wall wetting, and flow dynamics in the intake manifold, as shown in Figure 1. Spray modelling focuses on the spray formation and its spatial characteristics, such as liquid penetration length, Sauter mean diameter (SMD), cone angle, and jet velocity (Figure 2). Next, wall wetting is the outcome of the spray interacting with the engine's internal parts. The impinging spray may form a liquid wall film, which hinders the mixture formation and prevents the engine from operating normally. Especially in methanol engines, due to increased latent heat of evaporation, the wall film evaporation is significantly slower than in gasoline engines. Therefore, these wall deposits affect greatly the engine stability causing cyclic variations and limiting the increase of methanol energy fractions in converted methanol-diesel dual-fuel engines. Finally, the liquid droplets interact with the flow field of the intake manifold. This flow field is distinctive for each engine due to its design and geometrical features, and determines the degree of mixing.

Table 2. Experimental conditions.

Item	LP Case Liu et al. (2022)	HP Case Ghosh et al. (2020)
Ambient Pressure [bar]	2	3
Injection Duration [ms]	10	2.5
Injection Pressure [bar]	6	200
Injection Quantity [mg]	4.67 (estimation)	14.23 (estimation)
Ambient Temperature [°C]	25	103
Fuel Temperature [°C]	25	90 (estimation)
Nozzle Diameter [mm]	0.15 (estimation)	0.23

In an attempt to decouple the aforementioned modelling aspects, our study focuses on the spray modelling of PFI conditions. This paper provides a spray modelling framework that could be adapted to any specific 3D engine model (Figure 2). We validated the model specifically for methanol to operate robustly in a range of injection pressures in PFI ambient conditions. Coupling the framework with wall wetting models can serve as a valuable tool to study mixture formation, and identify the optimal retrofitting solution. CFD can provide a toolbox to study different injection pressures, injection locations and timings a priori. Eventually, these results demonstrate atomisation, evaporation, and jet velocity trends, which can provide insights into the required development direction for the technology of methanol PFI engines.

2.2. Experimental background

We selected two methanol spray experiments from the literature to validate our numerical models, which investigated methanol spray characteristics in CVC environments. These configurations were capable of offering controlled ambient conditions while allowing optical access for spray penetration and cone angle measurements. The experiments included a low injection pressure study (Liu et al. 2022), and a high injection pressure study (Ghosh et al. 2020), denoted as LP case and HP case respectively. For our study, we used liquid penetration data of these sprays under low ambient temperature and low ambient pressure conditions. These conditions match the intake manifold environment and are closely linked to the operating points of small-bore marine engines. The utilised experiments aimed to accommodate both low and high injection pressure in the engine intake manifold. The details of the experimental conditions for each case are presented in Table 2.

In the LP case, Liu et al. (2022) used backlight imaging and high-speed photography to capture the spray morphology of methanol in intake manifold conditions. The study deployed a 14-hole injector

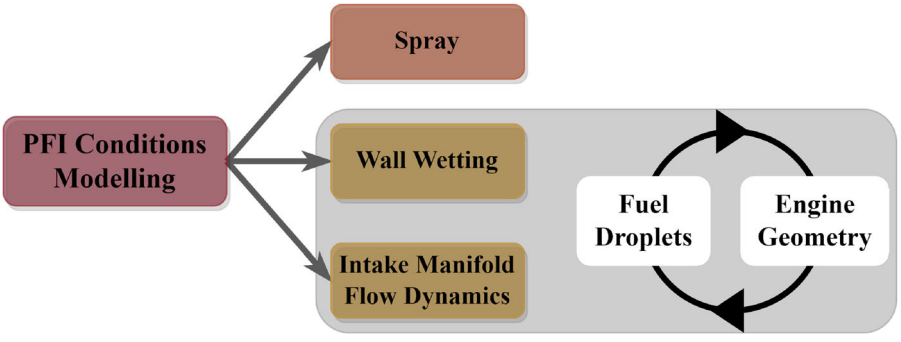

Figure 1. Schematic overview of modelling aspects for CFD modelling of PFI engines, demonstrating the decoupling of spray modelling, proposed in this work, from wall wetting effects and intake manifold flow dynamics, subject for future research.

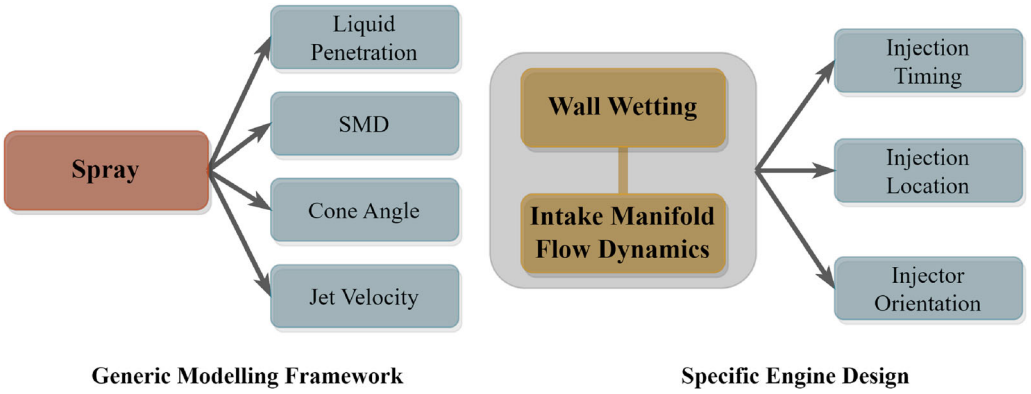

Figure 2. Pillars of PFI conditions modelling.

and investigated the influence of ambient temperature and pressure, and fuel temperature on spray penetration. The authors concluded that higher ambient and fuel temperatures induce flash-boiling, which result in faster evaporation time, and larger liquid penetration and cone angle.

On the other hand, in the HP case, Ghosh et al. (2020) employed a Mie-scattering technique via high-speed imaging to measure liquid penetration of methanol under a range of ambient pressures ranging from 3 to 40 bar. For our study, we used the 3 bar condition to validate our results. The elevated injection pressure was accomplished through a common rail DI style injector using a relatively large nozzle diameter (0.23 mm) with an L/D ratio of 4.9, suitable for heavy-duty applications.

Both of methanol experiments used light-duty and medium-duty automotive methanol quantities, which are orders of magnitude lower than marine injection. In the present numerical study, we used spray models that rely on non-dimensional fluid mechanics principles (Section 3). When scaled up, these models can produce physically rational conclusions. This is justified by previous research on diesel sprays, which reported that automotive-engine spray models can adequately predict the liquid penetration for marine engines (Li et al. 2021). Therefore, the CFD models can be validated through lower quantities and then scaled up for increased maritime quantities.

3. Computational methodology

The present study used the commercial CONVERGE v3.0 CFD software (Convergent Science; Senecal et al. 2012), which contains a numerical framework for multiphase flow simulations. The framework applies the finite volume method to solve the compressible conservation equations of mass, momentum, and energy (Convergent Science Inc 2022). We followed a RANS approach to model turbulence using the RNG and Standard $k-\epsilon$ models (Han and Reitz 1995). To solve the conservation equations, we used the density-based solver (Convergent Science Inc 2022) along with the Pressure Implicit with Splitting of Operators (PISO) algorithm (Issa 1986). Moreover, the numerical scheme's accuracy is first order in time and second order in space. For the determination of the time-step, we applied a control algorithm based on the Courant-Friedrichs-Lewy (CFL) criterion (Ferziger et al. 2002; Kundu et al. 2015; Convergent Science Inc 2022). The thermodynamic properties of both air and methanol were modelled based on the Redlich-Kwong equation of state (Horvath 1974). Lastly, the simulations were run in parallel on the DelftBlue supercomputer (Delft High Performance Computing Centre DHPC).

3.1. Computational domain & grid

A cylindrical geometry was adopted as the control volume for the numerical computations (Figure 3) with a 60 mm radius and 180 mm height. The dimensions of the geometry were chosen according to spray CFD literature (Maes et al. 2016; Li et al. 2021). For the boundary conditions, the cylinder walls were set as wall-type Neumann for both temperature and turbulent kinetic energy. For the meshing, CONVERGE generates the grid while the simulation is running through a modified cut-cell Cartesian technique (Senecal et al. 2007). The base cell size of the mesh is 4 mm with additional user defined and automatic refinements in areas of interest. Specifically, we refined the spray cone region to better resolve the flow field and the interactions between the droplets and the ambient air (Figure 3). This static mesh, however, is computationally expensive to implement in full engine simulations. An Adaptive Mesh Refinement (AMR) algorithm was used to keep the cell count low based on velocity and species gradients. Near the nozzle exit, a small refinement cone was also enabled for the sufficient resolution of the flow, while AMR refined the transient tip of the spray.

3.2. Spray model

To model the multiphase flow, we used the Lagrangian-Eulerian (LE) framework (Baumgarten 2006). The coupling uses a Lagrangian Particle Tracking (LPT) technique, which treats the liquid droplets as Lagrangian particles (Subramaniam 2013). The particles are tracked based on their position and motion in the computational domain. On the contrary, the gaseous phase is represented in a Eulerian way, which models the flow based on a mesh grid. In addition, a set of phenomenological spray models was used to resolve the physical phenomena that occur in the sub-grid length scales (Baumgarten 2006).

The computational parcels were injected using the Reitz and Diwakar (1987) model. The model assumes the initial discrete spherical droplets ('blobs') to be the same size as the nozzle diameter. These parcels interact with the surrounding air and breakup due to instability mechanisms. The breakup mechanism of each droplet is closely associated with the Weber (We) number, which is the ratio of the aerodynamic drag force imposed from the ambient air onto the droplet and the droplet surface tension force (O'Rourke and Amsden 1987):

$$\mathrm{We} = \frac{\rho_g u_r^2 d}{\sigma}, \tag{1}$$

where ρ_g is the ambient air density, u_r is the relative velocity between the droplet and the gas, d is the droplet diameter, and σ is the droplet surface tension. The droplet velocity is associated with the injection velocity, which is closely coupled to the injection pressure. Thus,

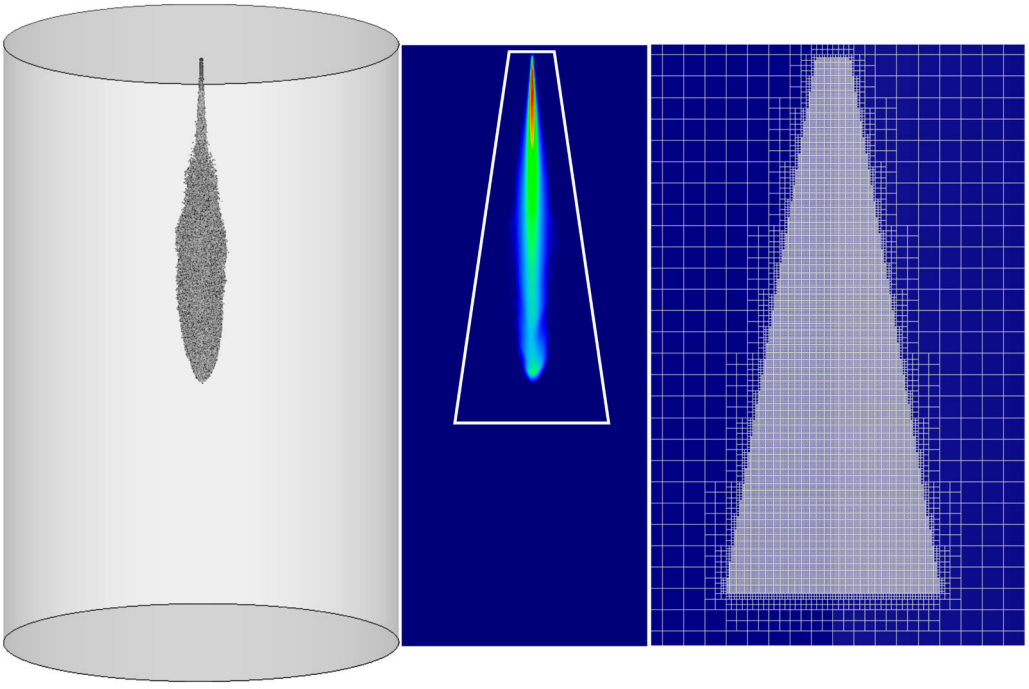

Figure 3. Simulation control volume: injected parcels, methanol mass fraction, and static cone mesh grid.

the different injection pressures used in this study require different breakup models due to altered breakup regimes. We used two separate droplet breakup models:

(1) Kelvin Helmholtz – Rayleigh Taylor (KH-RT) model, suitable for HP injection conditions (Reitz 1986; Beale and Reitz 1999).
(2) Taylor Analogy Breakup (TAB) model, suitable for low We number conditions (O'Rourke and Amsden 1987).

The KH-RT model is based on two separate mechanisms occurring during droplet breakup's primary and secondary phases. Kelvin-Helmholtz hydrodynamic instabilities dominate the primary breakup phase, attributed to the unstable shear waves of the droplet-air interface (Reitz and Diwakar 1987; Beale and Reitz 1999). Likewise, the secondary breakup is caused by the aerodynamic drag force between the droplets and the air on the tip of the spray, attributed to Rayleigh-Taylor instabilities (Reitz and Diwakar 1987; Beale and Reitz 1999). In the KH model, the resulting child droplet r_c is proportional to the wavelength Λ_{KH} of the fastest growing unstable KH surface wave (Beale and Reitz 1999):

$$r_c = B_0 \Lambda_{KH}, \tag{2}$$

where B_0 is the KH model size constant. The rate of change of the parent parcel radius r_p is calculated with the following expression:

$$\frac{\mathrm{d}r_p}{\mathrm{d}t} = -\frac{(r_p - r_c)}{\tau_{KH}}, \tag{3}$$

where the breakup time τ_{KH} is given by:

$$\tau_{KH} = \frac{3.726 B_1 r_p}{\Lambda_{KH} \Omega_{KH}}, \tag{4}$$

where B_1 is the breakup time constant, and Ω_{KH} is the growth rate of KH waves.

In the RT model, the breakup is inflicted due to the unstable waves, which are normal to the spray tip and originate from the deceleration of the droplets. Hence, the RT instabilities demonstrate growing wavelengths, which are dictated by the fastest wavelengths, similar to the KH instability (Beale and Reitz 1999):

$$\Lambda_{RT} = 2\pi \sqrt{\frac{3\sigma}{\alpha(\rho_l - \rho_g)}}, \tag{5}$$

where α is the deceleration of the drop, and ρ_g and ρ_l are the gas and liquid densities respectively. Similar to the KH model size constant in Equation (2), the RT model size constant C_{RT} dictates the wave sizes of the instability. If the length scale of the waves ($C_{RT}\Lambda_{RT}$) is larger than the parent drop diameter, breakup occurs. When the RT waves have grown for a sufficient time τ_{RT}, breakup will occur accordingly:

$$\tau_{RT} = \frac{C_\tau}{\Omega_{RT}}, \tag{6}$$

where C_τ is the RT breakup time constant, and Ω_{RT} is the growth rate of the waves.

In the case of LP injection, we used the TAB model, which assumes the droplet distortion and breakup to be proportional to a spring-mass-damper system (O'Rourke and Amsden 1987). The TAB model, however, is capable of tracking only one droplet breakup mode, for We < 12, which corresponds to the oscillation of droplets (Hsiang and Faeth 1995). This means that TAB breakup will occur only under LP injection (Zoumpourlos et al. 2023).

Marine engines require significantly larger nozzle diameters compared to automotive style injectors to provide the demanded fuel quantities. Thus, the near-nozzle Weber number of the droplets may be high enough to create KH instabilities instead of oscillating breakup modes. The nozzle-out theoretical Bernoulli velocity (u_{th}) of the jet is defined by the following expression (Payri et al. 2005):

$$u_{th} = \sqrt{\frac{2(P_{inj} - P_{amb}))}{\rho_f}}, \tag{7}$$

where P_{inj} is the injection pressure, P_{amb} is the ambient pressure, and ρ_f is the fuel density. Based on the critical Weber number (We = 12) and the nozzle-out Bernoulli velocity, the critical injection pressure P_{inj}^{cr} for a given nozzle diameter d is calculated as follows:

$$P_{inj}^{cr} = \frac{6\sigma}{d}\frac{\rho_f}{\rho_g} + P_{amb}, \tag{8}$$

where ρ_g is the ambient air density, and σ is the droplet surface tension. Depending on the nozzle diameter, the calculated critical injection pressure determines the most appropriate breakup model for the simulation. Hence, a lower injection pressure than the critical necessitates the use of the TAB model, whereas the KH-RT model must be used for higher injection pressures.

The spray droplets interact with each other through collisions and coalescence. The No Time Counter (NTC) algorithm (Schmidt and Rutland 2000) estimates the collisions between droplets, while the model of Post and Abraham (2002) predicts the post-collision outcome, including bouncing, stretching, reflective separation, and coalescence. Furthermore, the droplets interact with the surrounding gas through aerodynamic drag forces and turbulent flow phenomena. The droplet aerodynamic drag force was modelled with a dynamic drag model with the drag coefficient changing in relation to flow conditions (Liu et al. 1993). In the same model, the distortion of the droplet was also calculated using the TAB model calculations to secure a robust estimation of the drag coefficient.

A turbulent dispersion model was used to couple the turbulent flow of the gas with the lagrangian parcels (Amsden et al. 1989; O'Rourke 1989). We applied a Frossling correlation to predict evaporation phenomena, which assumes uniform temperature distribution within each droplet (Miller et al. 1998; Convergent Science Inc 2022). Finally, an additional boiling model was included to address the droplet radius change under boiling regimes (Convergent Science Inc 2022). A summary of the numerical models is listed in Table 3, and presented visually in Figure 4.

3.3. Model parameter selection

The details of the used submodel constants are presented in Table 4. Apart from the constants that are associated with the nozzle characteristics, the rest have been selected based on the guidelines provided by CONVERGE (Convergent Science Inc 2022). The same modelling constants were used for both high and low pressure injection cases to evaluate the robustness of the modelling framework. To validate the model, we conducted a sensitivity analysis on three modelling inputs: (i) the mass rate of injection (ROI) profile, (ii) the jet cone angle, and (iii) the turbulence model. Specifically, the ROI profile significantly affects the transient response of the spray. Uncertainties in the ROI prevent CFD modelling from accurately capturing the spray development (Pickett et al. 2013). Each injector has a unique profile, which needs to be measured experimentally and utilised in the CFD model (Payri et al. 2005). Given that the ROI profile for our case study remains undetermined, we conducted a comprehensive sensitivity analysis to assess its potential impacts, as detailed in Section 4. Thus, we justified the selection of the most appropriate profile for PFI conditions.

On the other hand, the cone angle influences the three-dimensional spray structure and the liquid penetration. Generally, a larger cone angle leads to lower liquid penetration due to increased air entrainment (Saha et al. 2017; Duronio et al. 2020). Detailed nozzle flow studies highlighted the importance of selecting a physically meaningful cone angle for spray simulations (Saha et al. 2017). For both injection pressure cases, we selected the cone angle according to the experimental results. Finally, the turbulence model greatly affects the interaction between the ambient gas and the resulting spray dynamics. We compared three different turbulence model cases, using the RNG $k-\epsilon$, the Standard $k-\epsilon$, and the Standard $k-\epsilon$ with a modification. This modification included the round jet correction, where we changed the $C_{\epsilon 1}$ constant to 1.55 (Pope 1978). This modification influences the production term of the TKE dissipation rate ε, and corrects the under-prediction of liquid penetration, which was observed in diesel sprays (Maes et al. 2016).

Since the injector characteristics were unknown, we calculated the nozzle discharge coefficient based on the Lichtarowicz et al. (1965) correlation. The correlation estimates the discharge coefficient based on the L/D ratio of the nozzle:

$$C_d = 0.827 - 0.0085 \cdot L/D \tag{9}$$

For the HP injection, the ratio L/D equalled 4.9, whereas, for the LP injection, it was unknown. Therefore, we kept the same value for the LP injection case. As the modelled conditions are barely evaporating and no mixing occurs, the discharge coefficient does not affect significantly the mixture formation making our parameter choice consistent. Particularly for the LP nozzle, we assumed a single nozzle injector with the same injection characteristics (i.e. cone angle and injection duration) as in the experiment. The estimated parameters (see Table 2) were selected to match the experimental spray structure and liquid penetration.

Table 3. Numerical models.

Physical phenomena	Numerical models
Fluid Flow	Navier Stokes, density-based solver (Convergent Science Inc 2022)
Turbulence	RNG and Standard $k-\epsilon$ model (Han and Reitz 1995)
Droplet Injection	Blob model (Reitz and Diwakar 1987)
Liquid Breakup	KH-RT model (Beale and Reitz 1999) & TAB model (O'Rourke and Amsden 1987)
Droplet Drag Force	Dynamic Drag Model (Liu et al. 1993)
Droplet Collision	NTC model (Schmidt and Rutland 2000)
Droplet Coalescence	Post Collision Outcome model (Post and Abraham 2002)
Droplet Turbulent Dispersion	O'Rourke (1989) model
Droplet Evaporation	Frossling correlation-based & boiling model (Convergent Science Inc 2022)

Table 4. Modelling parameters.

Breakup model	
KH Model size & breakup time constants	$B_0 = 0.61$, $B_1 = 10$
RT Model size & breakup time constants	$C_{RT} = 0.6$, $C_\tau = 1$
RANS Turbulence Model	
Standard $k-\epsilon$ constants	$C_\mu = 0.09$, $C_{\epsilon 1} = 1.44 - 1.55$, $C_{\epsilon 2} = 1.92$, $C_{\epsilon 3} = -1.0$
RNG $k-\epsilon$ constants	$C_\mu = 0.0845$, $C_{\epsilon 1} = 1.42$, $C_{\epsilon 2} = 1.68$, $C_{\epsilon 3} = -1.0$
Initial Turbulence Intensity	
Turbulent Kinetic Energy (TKE)	$k_0 = 1\,\mathrm{m^2/s^2}$
TKE Dissipation Rate	$\varepsilon_0 = 100\,\mathrm{m^2/s^3}$
Mass Diffusivity	
Methanol diffusivity constants	$D_0 = 1.336 \cdot 10^{-5}$, $n_0 = 1.8$
Nozzle Characteristics	
Cone Angle	LP-case: *known variable angle (initial value: 45°C)*, HP-case: 8°C
Discharge Coefficient	$C_d = 0.79$ (both cases)

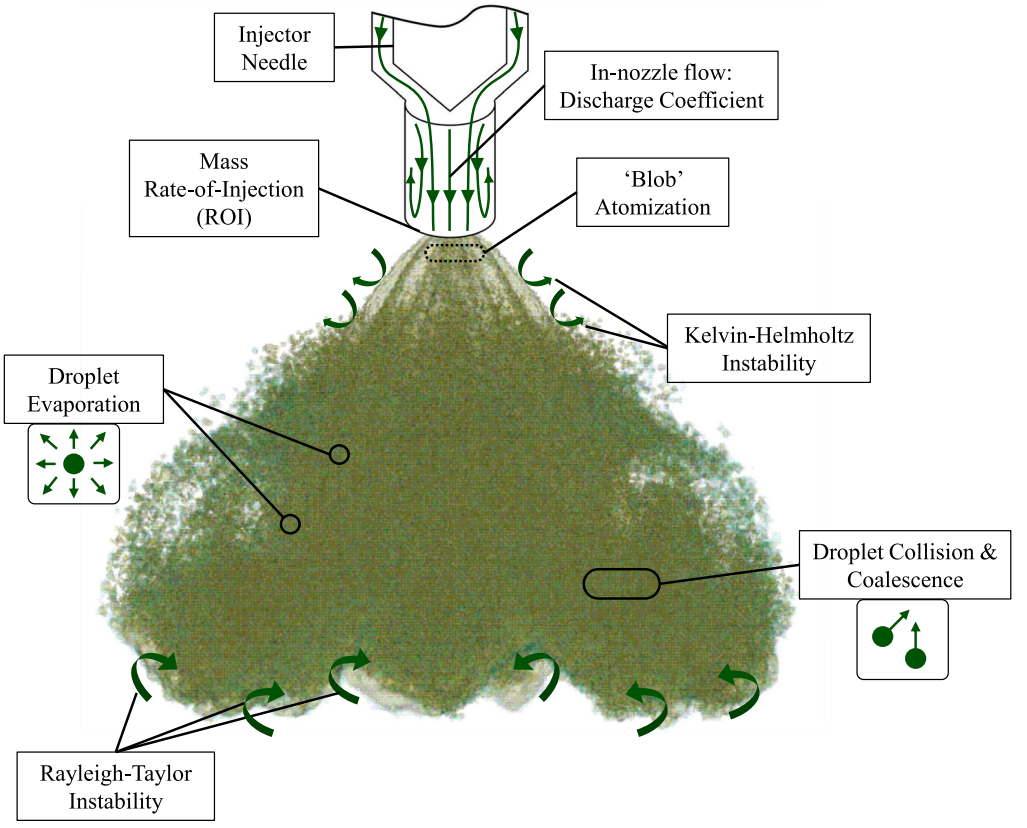

Figure 4. Schematic overview of the implemented spray modelling methodology.

In the LP case, the liquid penetration is defined as the vertical distance between the nozzle and the identified spray edge (Liu et al. 2022). In the HP case, the authors followed the ECN guidelines by employing a Mie-scattering technique to measure liquid penetration (Ghosh et al. 2020). In the numerical results, the liquid penetration was calculated by a 95% threshold for the liquid mass fraction. Although an inherent difference exists in the liquid penetration definition between our model and the experiments, we consider it negligible for the scope of the present study. A more strict comparison has been achieved by the ECN for gasoline sprays (Spray G). However, these investigations included more detailed experiments using diffused back-illumination, Mie-scattering, and PIV techniques (Sphicas et al. 2017; Hwang et al. 2020; Paredi et al. 2020). Lately, the ECN has conducted dedicated methanol spray studies using an ECN spray style multi-hole injector (Spray M). Although the experiments mainly focussed on gasoline direct injection engines, future research could investigate heavy-duty and PFI applications. In our study, we accept the existing liquid penetration data, which are dedicated for methanol, for our numerical investigations.

4. Results & discussion

4.1. Simulation plan

The present study followed a structured simulation plan to construct a predictive framework for marine PFI sprays. The mesh size was initially analysed by comparing a static and an automatically refined mesh grid. After investigating the mesh influence, we performed a set of simulations to demonstrate the sensitivity of each input parameter on liquid penetration. The parameters include the mass ROI, the cone angle, and turbulence model, as mentioned in Section 3.3. Consequently, we compared their influence with the experimental data and highlighted the importance of assigning realistic values in the model. Based on the outcomes of the sensitivity analysis, we selected a baseline model and scaled up the injected mass to account for marine engine operation. The marine case study explored the influence of the injection pressure on breakup, evaporation, and jet velocity, as well as the impact of the ambient environment conditions on spray penetration. In Figure 5, we provide a visual representation of the implemented simulation plan.

4.2. Mesh size influence

For the mesh sensitivity analysis, we used four different mesh grid sizes for each injection pressure. Three cases involved a static mesh with a refinement in the cone shaped area as shown in Figure 3, and a single AMR case with a dynamically changing grid. The refined cells were sized as 1 mm for the coarse mesh, 0.5 mm for the medium mesh, and 0.25 mm for the fine mesh cases. In the AMR case, we followed the same approach with the fine grid by using a small cone refinement close to the nozzle exit. The AMR algorithm refined the evolving spray tip with a minimum cell size of 0.25 mm. Subsequently, we compared the AMR case with the static mesh cases in terms of computational accuracy and cost. In Table 5, we present the mesh grid parameters including the total cells and computational cost for each computational grid. The LP case exhibits a higher cell count because the larger cone angle of the experiment required an increased cone refinement area.

In the present section, the baseline models were selected for the mesh sensitivity analysis with the parameters presented previously in Table 4. Moreover, we considered a top-hat ROI profile and the modified Standard $k-\epsilon$ for both LP and HP injection cases. In Figure 6, the resulting liquid penetrations are presented for both

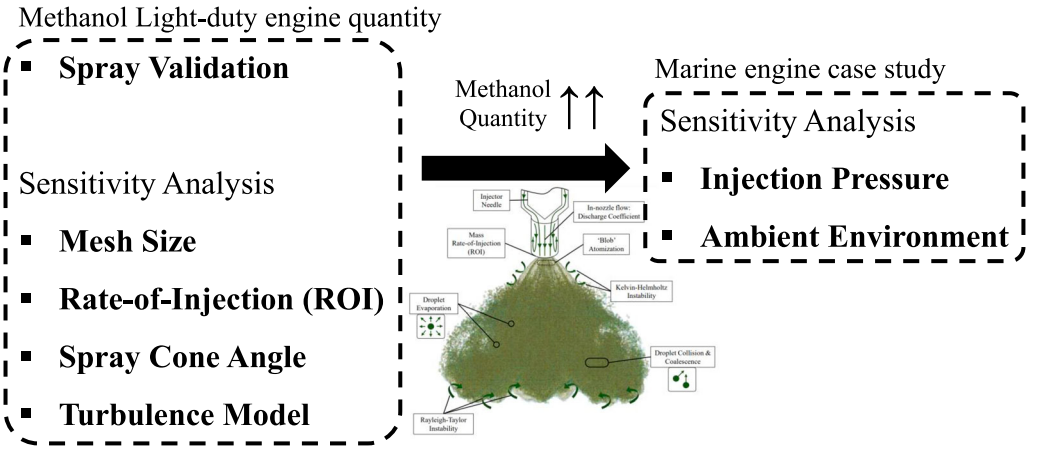

Figure 5. Overview of the conducted simulation cases.

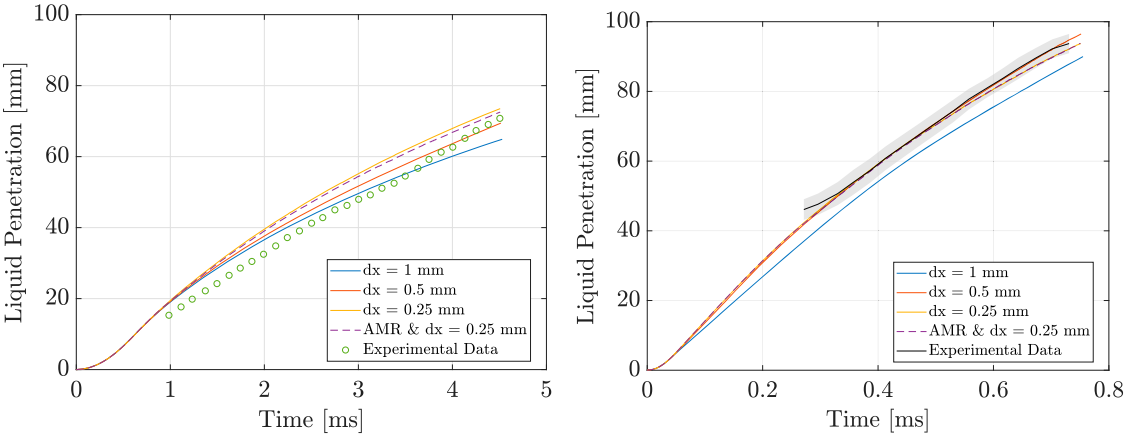

Figure 6. Mesh size effect on liquid penetration. (a) Low Pressure Injection. (b) High Pressure Injection.

Table 5. Mesh grid parameters for Low Pressure (LP) and High Pressure (HP) injection.

	Minimum cell size [mm]	Cell count [−]	Computational cost [core-hours]
LP coarse	1.0	0.17 *M*	0.15
LP medium	0.5	1 M	1.8
LP fine	0.25	7.7 *M*	32.9
LP AMR	0.25	0.06 *M*	0.19
HP coarse	1.0	0.1 *M*	0.13
HP medium	0.5	0.5 *M*	0.75
HP fine	0.25	3.4 *M*	9.96
HP AMR	0.25	0.5 *M*	1.1

LP and HP cases. Higher injection pressure augments the penetration rate, due to the increased jet velocity. As a result, the entire spray process is faster than in the low injection pressure case. The results demonstrated that the model predicts the liquid penetration trends satisfactorily within the experimental uncertainty limits for both injection cases.

Mesh convergence was achieved for the fine grid in both cases for a mesh size of 0.25 mm. Particularly in the LP case, a previous study using the same model employed a computationally expensive 0.125 mm grid to further demonstrate the convergence of the 0.25 mm grid (Zoumpourlos et al. 2023). The CFD model captured well the trends of the experimental data ensuring a physical representation of the spray momentum. For both cases, the coarse grid under-predicted the liquid penetration, which aligns with trends that have also been observed in conventional fuels (Senecal et al. 2012). Interestingly, the AMR solution demonstrated similar results as the static mesh, but at significantly lower computational cost (more than 95% cheaper simulations). This aligned with Abraham (1997), who claimed that, for accurate spray predictions, cell resolution has to be on the order of the orifice diameter. Thus, the AMR grid was selected as the optimal grid for our numerical study ensuring a computationally affordable and accurate solution, which can be implemented in full engine models.

4.3. CFD framework parameter investigation

In this section, we analyse the sensitivity of the baseline model with the AMR grid from the previous section for both LP and HP injection, examining mass ROI, cone angle, and turbulence model. The decoupled effects of each parameter are then reported and compared. In each case, we altered the parameter of interest (i.e. ROI, cone angle, and turbulence model) while using the baseline model, as reported in the mesh sensitivity study. This comparison highlights the importance of these choices in spray modelling for marine engines. Ultimately, the sensitivity analysis strives to provide a solid foundation for the proposed modelling framework.

4.3.1. Rate of injection

Normally, individually for each injector, the ROI profile is generated by mass flow rate and momentum measurements which represent the hydraulic behaviour of the nozzle (Payri et al. 2016). Since the ROI is unknown for the employed injectors, a modelling convention is crucial for a realistic spray outcome. This paper aims to address this challenge by introducing an empirical ROI profile that can accurately predict the experimental liquid penetration, while representing the injection conditions. The profile is based on a top-hat style profile with a modified initial transient overshoot associated with the initial needle-lift overshooting motion. This represents the overshoot observed in the Spray G profile in low ambient pressure conditions in gasoline injection (Spray G). This overshoot is lower in the LP case due to low ambient and injection pressure. Conversely, the overshoot is more pronounced in the HP case because of the increased initial jet momentum coming from the high injection pressure. The normalised mass ROI profiles are presented in Figure 7. Along with the proposed top-hat profiles, we compared the Spray G profile, which is closer to the HP condition, a constant mass flow profile, and a CMT-generated profile from the online 'Virtual Injection Rate Generator' tool (CMT – Clean Mobility & Thermofluids Website).

Figure 8 illustrates the liquid penetration results for the LP injection case for each ROI profile. For all the simulated cases, the model over-predicted the experimental values due to the inherent uncertainty of the injector details. Thus, to mitigate this over-prediction, the model requires more accurate information on the nozzle diameter, discharge coefficient, and nozzle-hole topology. Despite this, the majority of the profiles provide reasonable predictions for the transient behaviour of the jet with less than 10% deviation from the experimental values. This highlights that sprays in LP injection conditions are insensitive to ROI variations in the scope of PFI modelling. Hence, our model demonstrates a satisfactory acceleration and initial momentum of the spray and predicts acceptably the liquid penetration.

Similar trends are also observed under HP injection in Figure 9, where the liquid penetration is within the experimental uncertainty range. Despite that, the CMT tool over-predicts penetration, similarly as in diesel injection studies (Pickett et al. 2013). This is probably attributed to the fact that the CMT tool was developed for diesel injection under high ambient pressure environments. Under these conditions, the injector needle overshoots less due to higher resistance forces originating from the higher ambient pressure environment. These forces impede the needle motion, and contrary to low ambient pressure injection, the injector needle displacement experiences lower overshoot.

4.3.2. Cone angle

The spray cone angle influences the liquid penetration and the jet morphology (Zembi et al. 2023). By tuning it appropriately, the spray structure can be accurately captured (Saha et al. 2017). In Figure 10, the comparison of 8, 10, 12, and 16 degrees of cone angle for the HP

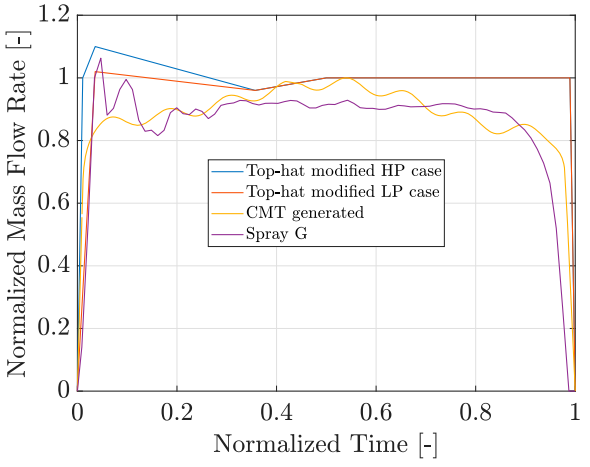

Figure 7. Mass ROI profiles (normalized over total injected mass).

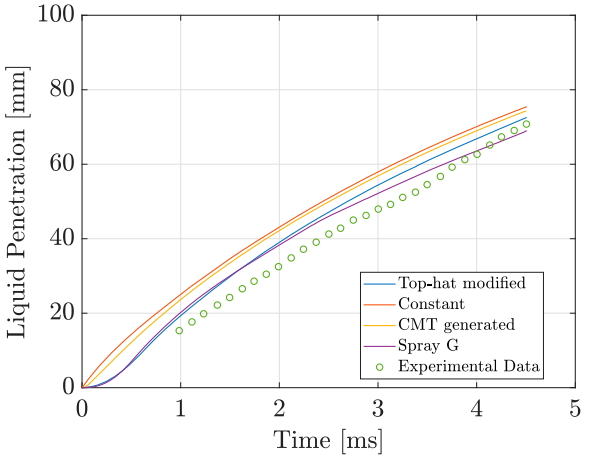

Figure 8. ROI profile influence on LP injection.

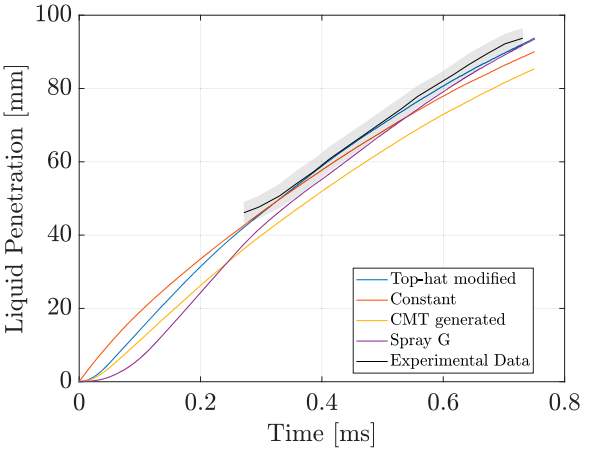

Figure 9. ROI profile influence on HP injection.

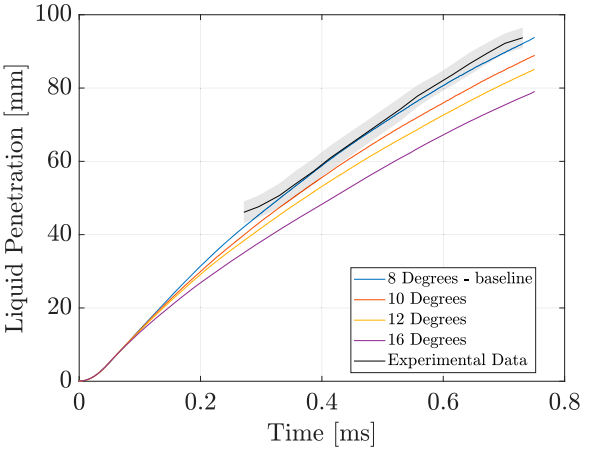

Figure 10. Cone angle influence on HP injection.

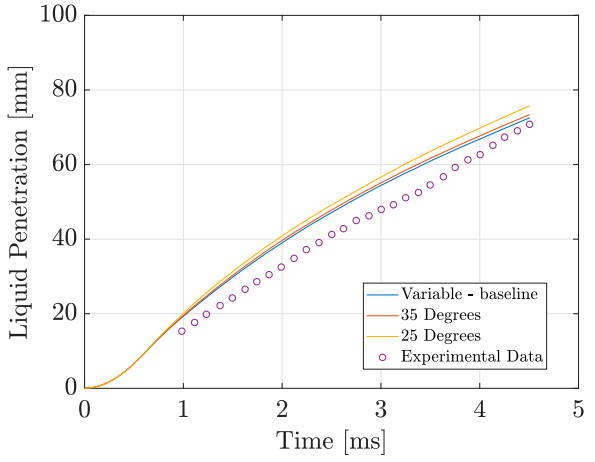

Figure 11. Cone angle influence on LP injection.

case confirms the large influence in liquid penetration. Hence, with even 2 degrees of perturbation in cone angle input, liquid penetration results are affected significantly. Thus, high pressure injection simulations need to be assigned with a realistic value for the cone angle. Small perturbations of this parameter can lead in imprecise mixture formation predictions due to incorrect liquid penetration.

Figure 11 depicts the cone angle influence for the LP case. Here, the different injector geometry requires larger cone angle values as input for the model. Contrary to the HP case, under low injection pressure, the cone angle slightly affects the liquid penetration, even for a wide range of jet angles (25 degrees, 35 degrees, and time-variable cone as reported by the experimental paper). This phenomenon is attributed to the low entrainment velocity that the LP injection jet experiences. Since the velocities are diminished, the jet does not entrain sufficient air to its core. Therefore, the momentum of the droplets is similar for any given jet cone angle, and the liquid penetration remains unaffected. Additional discussions on the entrainment velocity are conducted in Section 4.4.

4.3.3. Turbulence model

Figure 12 shows the liquid penetration results for the different turbulence model cases. As mentioned in Section 3.3, the turbulence model selection is affecting the ambient flow and spray formation. In the LP case, the effect of turbulence is not significant indicating low turbulent intensity. On the contrary, in the HP case, the Standard $k-\epsilon$ model significantly under-predicts the liquid penetration aligning with high injection pressure spray literature (Maes et al. 2016; Paredi et al. 2020; Zembi et al. 2023). The turbulence modification is justified as the axisymmetric nature of the spray cannot use default turbulence model constants, which are typically found in boundary layer flows (Pope 1978). In addition, the RNG $k-\epsilon$ model performs similarly to the modified Standard $k-\epsilon$, indicating its suitability for spray and combustion simulations in ICE models.

4.3.4. Sensitivity of modelling parameters

The sensitivity of each modelling parameter is presented in Figure 13. The figure presents the relative error between the final data point of the experiments and the associated worst-case result from the CFD model. For the HP case, all of the investigated parameters exhibit significant influence in the liquid penetration prediction. Specifically, the cone angle sensitivity is the highest among the ROI and selection of turbulence model. Thus, we conclude that uncertainties in cone angle and ROI during the modelling process could lead to large discrepancies in the outcome spray structure. Eliminating these uncertain parameters through experimental data or, if possible, tuning them realistically is mandatory for methanol engine simulations. On the other hand, in the LP case, the induced sensitivity is lower, due to the decreased intensity of the phenomena under low injection pressures. Lower droplet velocities inevitably result in reduced droplet breakup and evaporation, and thus, the studied changes have minor effect on the model predictions.

Finally, to demonstrate the predictive capabilities of the present framework, Figure 14 presents the liquid penetration of the HP case under varied experimental ambient pressure and temperature environments. For the increased ambient pressures, the experimental paper reported a proportional increase in ambient temperature, which promoted evaporation phenomena. As a result, the successful reproduction of the experimental results demonstrates the robustness of the present modelling framework.

4.4. Marine engine case study

To account for marine engine fuel quantities, we increased the injected mass and conducted a case study on the effect of injection pressure on methanol sprays. Consequently, we compared the outcome spray characteristics for each injection pressure. The evaluation

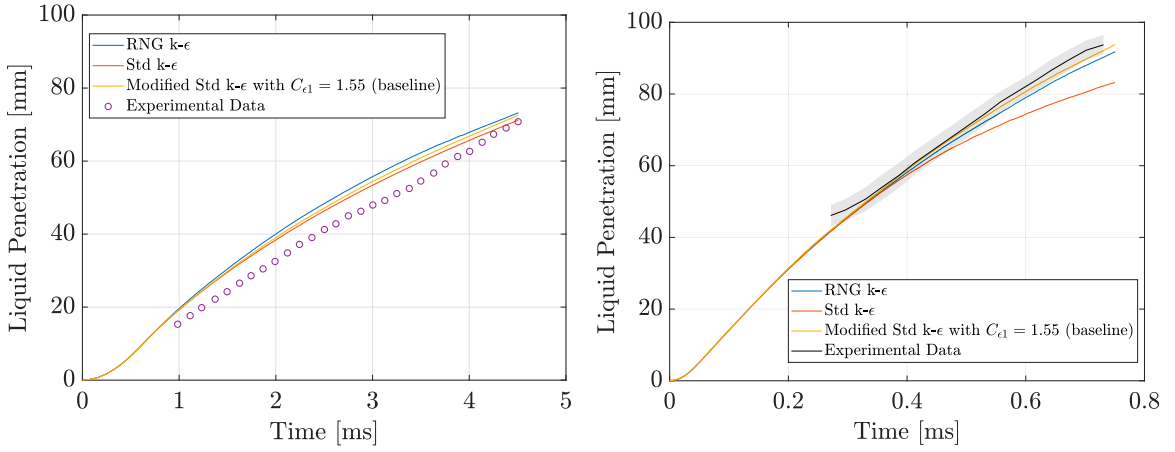

Figure 12. Turbulence modelling effect on liquid penetration. (a) Low Pressure Injection. (b) High Pressure Injection.

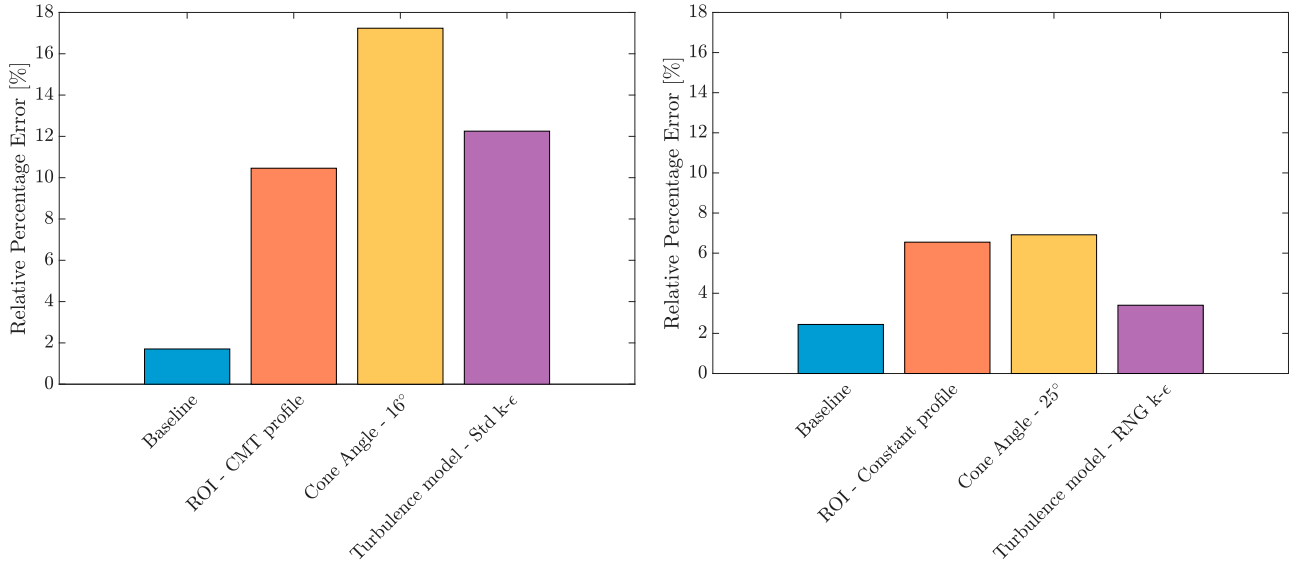

(a) HP injection sensitivity comparison (b) LP injection sensitivity comparison

Figure 13. Sensitivity of modelling parameters on predicted liquid penetration: comparison of ROI, cone angle, and turbulence model. (a) HP injection sensitivity comparison. (b) LP injection sensitivity comparison.

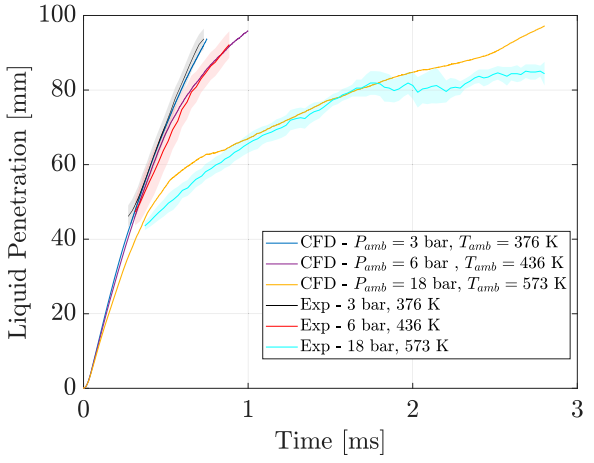

Figure 14. Validated HP model predictions at varying ambient pressures.

Table 6. Marine case study conditions.

Item	Value
Ambient Pressure [bar]	2
Ambient Temperature [°C]	100
Fuel Temperature [°C]	90
Injection Quantity [mg]	400
Nozzle Diameter [mm]	1.0

Table 7. Marine case study: injection pressure & duration.

Injection pressure [bar]	Injection duration [ms]
6	22.5
8	19.5
10	17.5
15	14.3
20	12.4
30	10.1
40	8.7
50	7.8
100	5.5
200	3.9

included the liquid penetration results, the breakup occurrence (in terms of spray SMD), and the entrainment velocity field. A larger nozzle diameter was used to replicate small-bore marine engine conditions to facilitate the increased methanol quantity. In Table 6, the ambient conditions are reported along with the details of injection quantity and nozzle diameter. The chosen conditions represent a small-bore marine engine, which was retrofitted for methanol PFI in previous research by our group (Bosklopper et al. 2020). In addition, Table 7 shows each case's injection pressure and associated injection duration. For each injection pressure, the injection duration was calculated to facilitate the predefined 400 mg of methanol. For the analysis, we used the validated modelling framework with the baseline parameters from the previous section (Section 4.3). The meshing strategy was the same as previously but with a minimum cell size of 0.5 mm due to the larger nozzle diameter. Similarly as in Section 4.2, we achieved mesh convergence for the 0.5 mm AMR grid through testing three different cell sizes ranging from 2 to 0.5 mm.

To prevent fuel impingement on the computational domain walls, the simulations were run until 25% of the fuel quantity was injected. While less fuel was injected during the simulation duration, we maintained a mass flow rate corresponding to 400 mg of methanol. Figure 15 demonstrates the resulting liquid penetration for the range of injection pressures. For high injection pressures, the spray penetrates faster determining the conditions prior to the wall impact. Nevertheless, similar liquid penetration is observed for the same injected quantity. Figure 16 depicts the advantage of higher injection pressures in terms of droplet breakup. Moreover, the spray SMD results demonstrate that significant improvements in droplet atomisation are realised by using high injection pressures.

With improved atomisation, the droplets have an increased effective area, which interacts with the surrounding gaseous medium and, thus, experiences faster evaporation. In Figure 17, we illustrate a spatial comparison of the droplet diameter for each injection pressure at the moment that 25% of the fuel quantity was injected. The spatial comparison shows that low injection pressures (<20 bar) have a higher concentration of droplets sized between 104 and 216 μm.

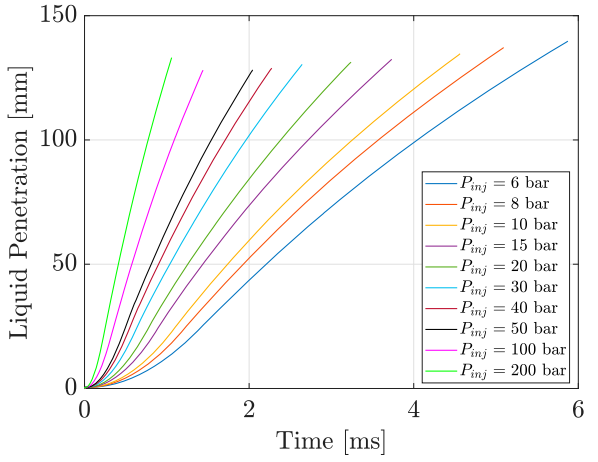

Figure 15. Effect of injection pressure on liquid penetration in marine PFI conditions.

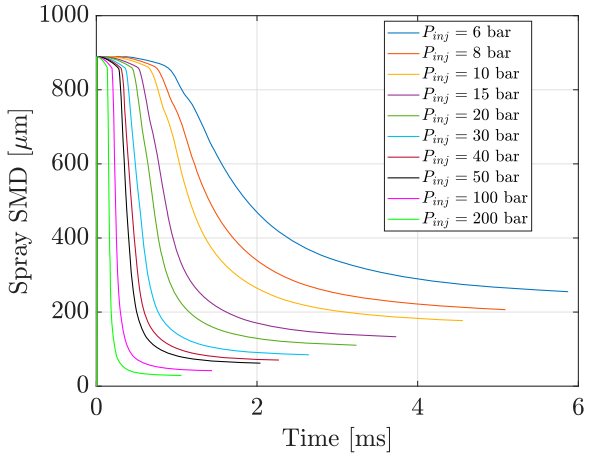

Figure 16. Spray SMD under different injection pressures.

On the other hand, for injection pressures higher than 50 bar, atomisation is enhanced with smaller droplets even in the vicinity of the spray.

The resulting evaporated methanol is presented in Figure 18. The 200 bar case exhibits the highest evaporated quantity confirming improved atomisation in increased injection pressure. The evaporation rate is also substantially increased, whereas for the low injection pressures evaporation is minimal. Nonetheless, when compared with the total injected mass, the total evaporated quantities are up to 1% (Figure 19). Hence, evaporation will be minimal at intake port conditions, as most of the fuel will impact the walls or the intake valve geometry. These findings indicate that the mixture formation may be dominated by wall film and in-cylinder evaporation phenomena.

The velocity vectors for each injection pressure are shown in Figure 20 for the moment that 25% of the fuel quantity was injected. Low injection pressures create very low air entrainment, while the core maintains a high momentum due to increased spray density. On the contrary, under high injection pressure, the spray velocity and air entrainment effects are an order of magnitude higher than in lower injection pressures. This results in a more diluted spray core with less momentum and higher droplet breakup. Additionally, under high injection pressure, the wing tip vortex is located closer

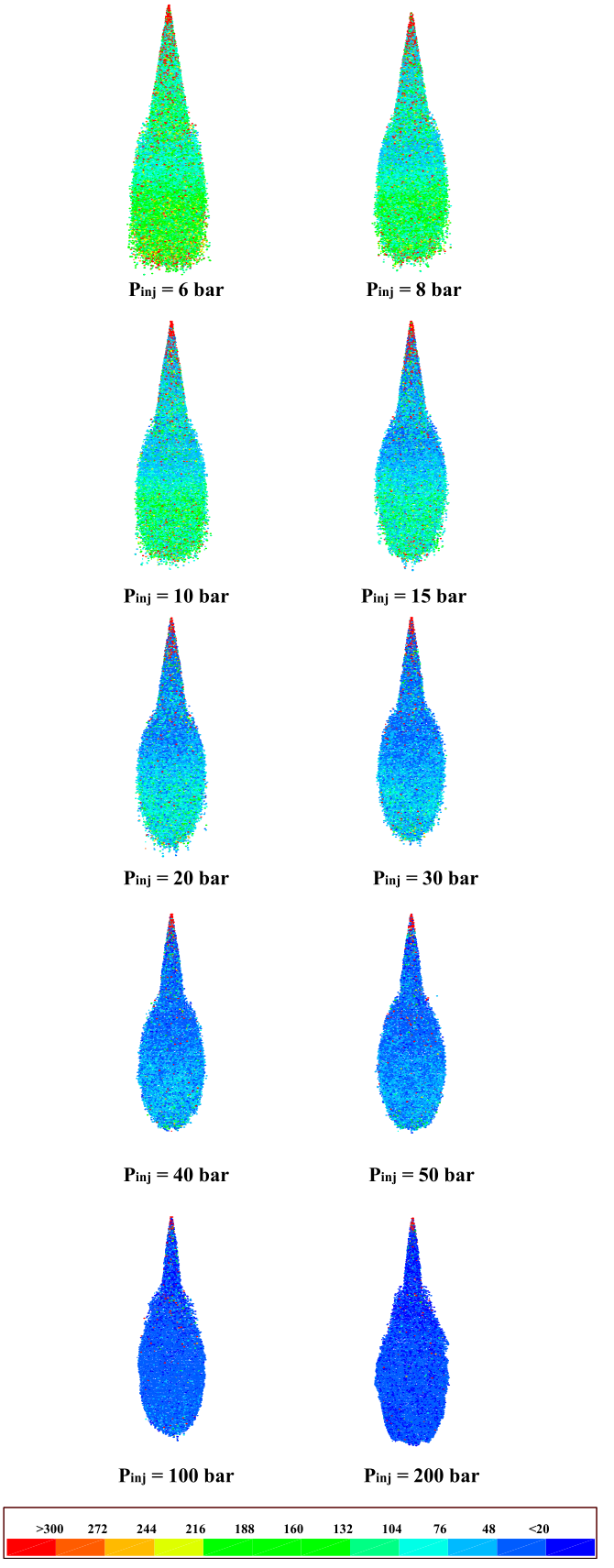

Figure 17. Droplet diameter (in μm) for each injection pressure.

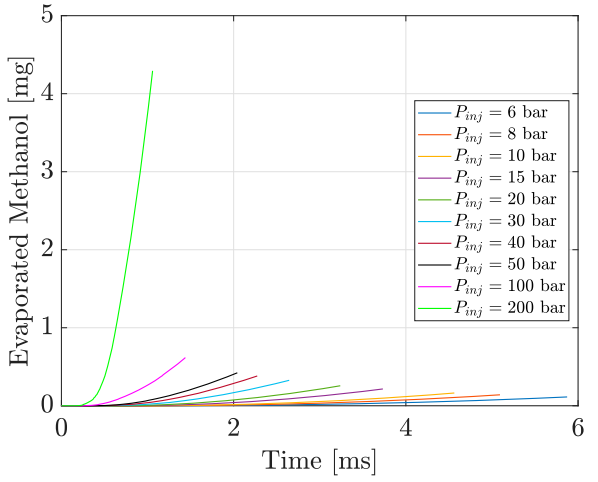

Figure 18. Evaporated methanol for each injection pressure.

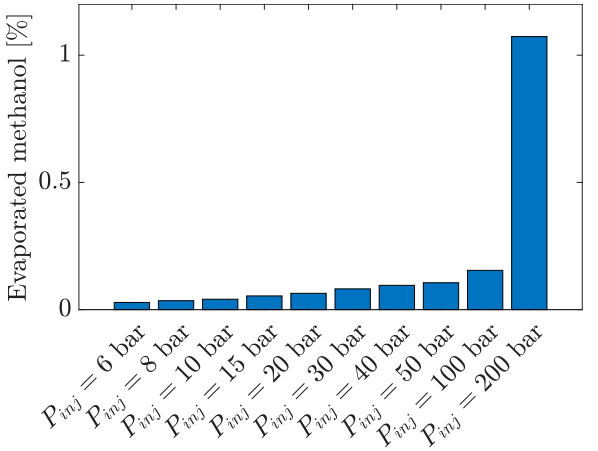

Figure 19. Percentage of evaporated methanol with respect to total injection quantity.

to the tip of the spray. Figure 21 displays the velocities in the vicinity of the spray and close to the nozzle exit (air entrainment point). Under low injection pressures (<30 bar), the air is entrained with less than 5 m/s, which is insufficient for the primary breakup of the jet. Similarly, the low injection pressures demonstrate low momentum indicating the decreased penetration rate shown in Figure 15.

Finally, Table 8 presents the nozzle tip *We* number for each injection pressure. For all the injection pressures, the droplets remain in the multimode and shear breakup regime (Hsiang and Faeth 1995). Even with low injection pressures, primary breakup is predicted correctly using the KH model, because marine nozzle dimensions produce sufficiently large droplets. These large droplets exhibit increased We numbers with higher injection pressure than the critical, remaining outside of the oscillation and deformation breakup regimes. However, automotive-style nozzles in PFI conditions may require the TAB model to predict breakup as the droplets lie within the oscillation breakup regime (Zoumpourlos et al. 2023).

4.4.1. Influence of ambient environment on marine PFI sprays

In this section, we conduct a sensitivity analysis on the ambient pressure and temperature, and report their effect on the spray. For the present investigation, we used the previous marine injection conditions reported in Table 6 along with a fixed injection pressure of

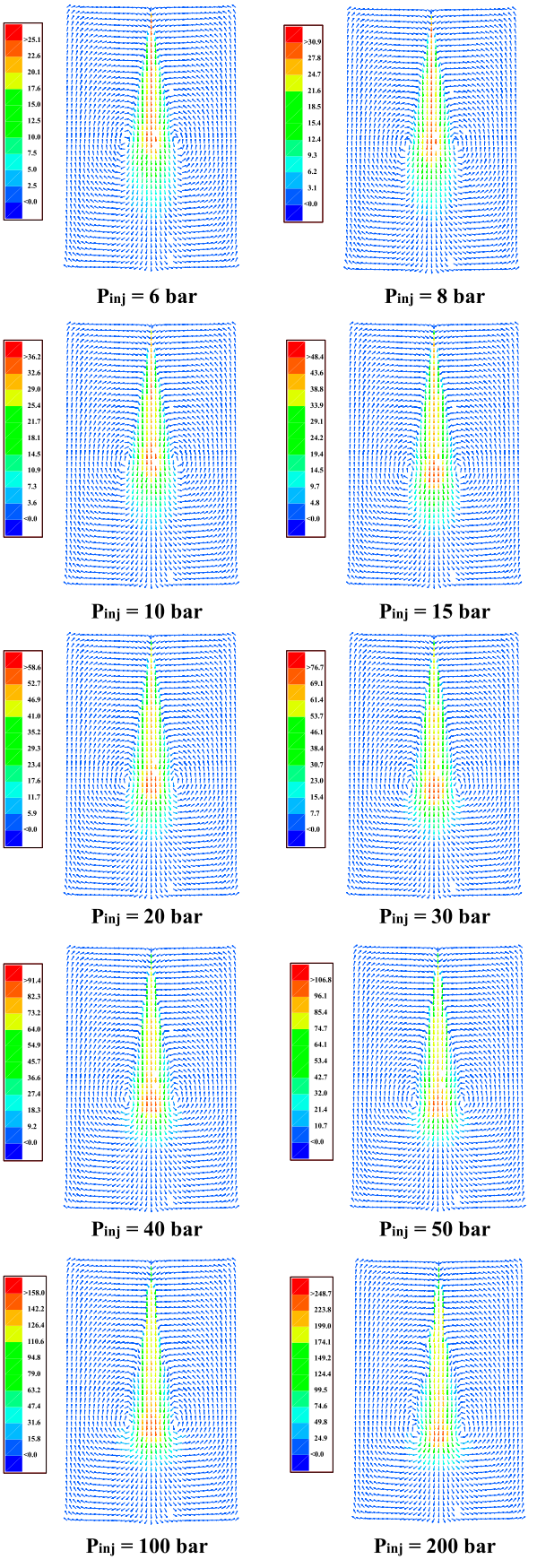

Figure 20. Entrainment velocity vectors for each injection pressure.

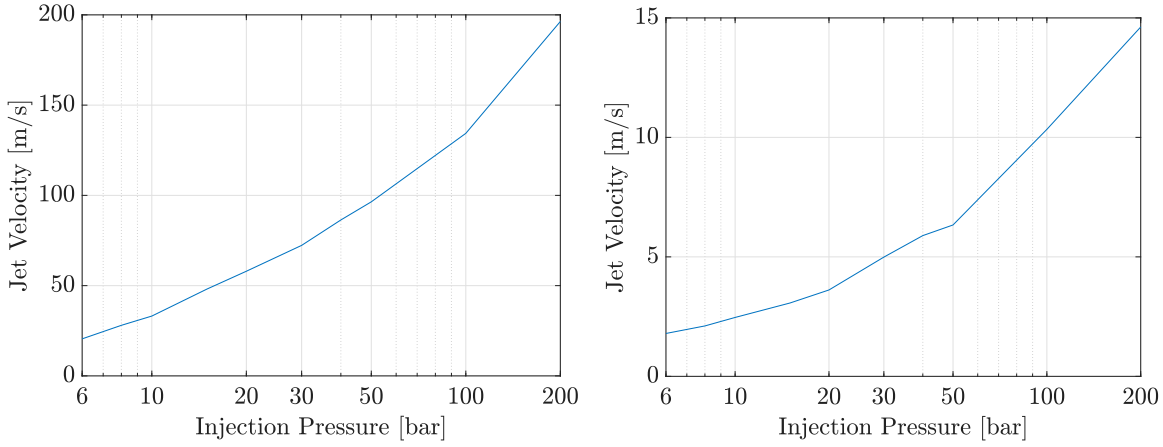

(a) Jet velocity for each injection pressure at $z = 100$ mm point

(b) Entrainment velocities for each injection pressure at $z = 14.5$ mm and $y = \pm 3.5$ mm (average of $y = \pm 3.5$ mm points)

Figure 21. Injection pressure effect on jet velocity. (a) Jet velocity for each injection pressure at $z = 100$ mm point. (b) Entrainment velocities for each injection pressure at $z = 14.5$ mm and $y = \pm 3.5$ mm (average of $y = \pm 3.5$ mm points).

Table 8. Nozzle exit weber number.

Injection pressure [bar]	We number [−]
6	50
8	68
10	85
15	123
20	170
30	260
40	350
50	430
100	850
200	1650

10 bar. Figure 22 depicts the influence of ambient pressure on liquid penetration and SMD. For the low ambient pressure cases, the spray exhibited increased penetration and SMD due to the lower drag forces imposed on the droplets' surface. In the case of high ambient pressure, higher drag forces augmented the droplet breakup occurrence leading to decreased penetration and SMD. Furthermore, Figure 23 illustrates the ambient temperature sensitivity analysis. Higher ambient temperatures lower the ambient density, and as a result, both the liquid penetration and SMD are slightly increased proportionally. This is valid while the spray is outside of the flashing regime, which in the presented cases is true. Thus, with the modification of the ambient conditions, the CFD model could provide physically accurate predictions.

5. Conclusions

In this paper, we presented a CFD framework, which uses state-of-the-art spray modelling to reproduce methanol sprays under PFI conditions with a well-established approach for diesel and gasoline. These conditions are characterised by low ambient pressure and temperature and low injection pressures (ranging from 6 to 10 bar), often found in four-stroke medium- and high-speed marine engines operating with premixed methanol combustion. To overcome the challenges of poor atomisation, our framework was extended to higher injection pressures up to 200 bar. Our work is the first to use methanol experimental data for both high and low injection pressures to validate and tune the models for robust operation in PFI conditions. We investigated the sensitivity of the uncertain parameters caused by the unknown injector specifications on liquid penetration. The validated model was then applied in a marine engine case study, using increased methanol quantities, and demonstrated the evaporation and atomisation challenges in PFI conditions.

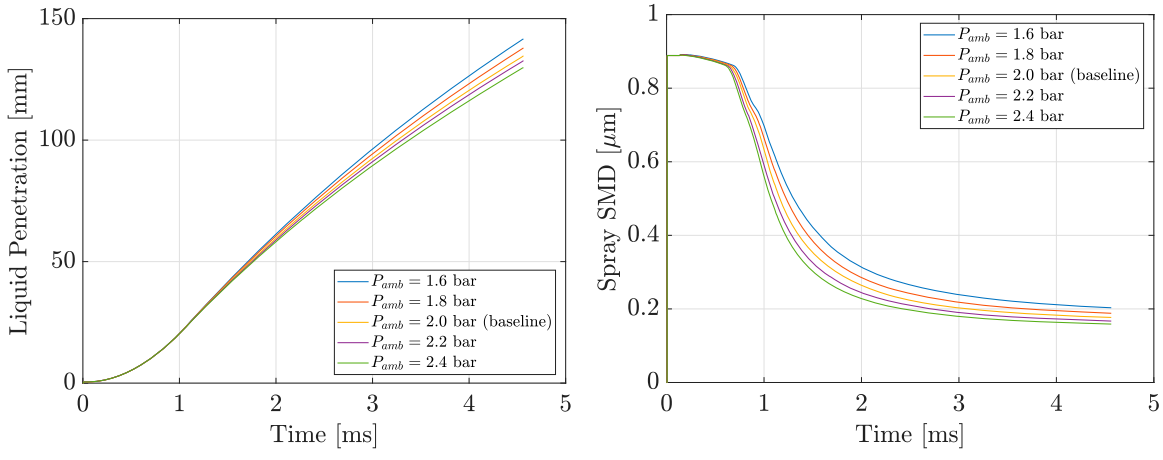

Figure 22. Influence of ambient pressure on liquid penetration (left) and SMD (right) for 10 bar injection pressure.

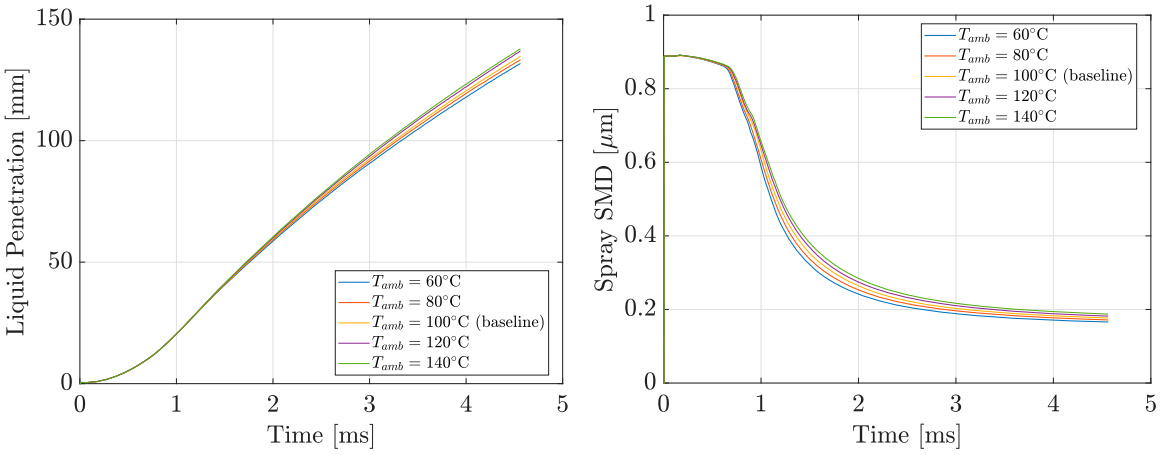

Figure 23. Influence of ambient temperature on liquid penetration (left) and SMD (right) for 10 bar injection pressure.

Based on the model results, we found several key insights. The sensitivities of mesh, ROI, cone angle, and turbulence model have been thoroughly investigated and reported. Resolving the flow with AMR is the most efficient way to simulate engines in CFD environments. We demonstrated that with an unknown ROI, a modified top hat profile with an initial transient response yields satisfactory results for both high and low injection pressures. Accurate spray predictions necessitate a precise definition of the cone angle, as it significantly influences the spray structure. Under low injection pressure conditions, the effects of cone angle and turbulence are negligible, whereas under high injection pressure, the modified Standard and RNG models perform as expected. This is due to increased droplet velocities, making HP injection highly sensitive to ROI and cone angle inputs.

In contrast, for low-pressure (LP) injection, the jet velocity is significantly lower than in high-pressure (HP) scenarios, resulting in the spray structure and the adjacent flow phenomena having a lesser impact on the in-cylinder mixture formation. Consequently, evaporation and mixing may be more influenced by wall wetting phenomena. This suggests a potential area for further research, which could involve exploring the coupling of the current framework with wall wetting models to investigate mixture formation in intake port manifold environments. Additionally, there should be a focus on studying wall wetting evaporation parameters, like film thickness and size, in associated marine engines. For small injection quantities typical of automotive style, the low jet velocity also influences the applicability of the droplet breakup model. Thus, for an injection pressure lower than a critical value, the TAB model should be implemented for accurate liquid penetration predictions.

Following the spray model validation, we scaled up the injected methanol quantity to 400 mg using a larger single-hole nozzle. The simulated conditions aimed to account for a marine engine operating with methanol premixing at the intake manifold. Using the scaled up marine engine injection model, we performed a case study encompassing a set of different injection pressures ranging from 6 to 200 bar. Subsequently, using the 10 bar injection pressure case, we conducted a sensitivity analysis on the ambient conditions, and revealed the isolated effect of ambient pressure and temperature on spray penetration. Using higher injection pressures results in the spray jet breaking up faster, which promotes evaporation and improves mixture formation. However, evaporation occurring at the initial stage of injection, before impact with the wall, is minimal. Therefore, higher jet velocities will evidently affect wall wetting in conjunction with the cross-flow of the inlet manifold. This pattern is similar to what is observed in LP injection, indicating that wall wetting effects may still dominate. Studies of conventional fuels have not produced consistent results about the influence of injection pressure on wall wetting (Duronio et al. 2020). This suggests a need for additional experimental and simulation work in this area, which will reveal the interaction between spray and intake air cross-flow in the intake manifold.

In summary, injection pressure dictates atomisation and pre-wall impact conditions, as ambient temperature in PFI environment is load dependent. Higher injection pressures can potentially overcome methanol evaporation challenges, as could alternative injection hardware. This study provided a best-practice for the CFD analysis of injection timing and location for real engine geometries under a wide range of injection pressures. When coupled with wall-wetting models, our approach can identify the challenges of methanol marine engine conversion. CFD simulations can be an important step towards robust methanol operation and, eventually, assist in accomplishing sustainability targets.

Acknowledgments

The present research is part of the MENENS project (Methanol als Energiestap Naar Emissieloze Nederlandse Scheepvaart). We would like to thank Convergent Science (Convergent Science), and BETA CAE Systems (BETA) for offering their software (CONVERGE, ANSA & META) and their technical support for the accomplishment of this research. ANSA was used for geometry creation and pre-processing of the CFD model, CONVERGE for the CFD simulations, and META for post-processing and visualisation of the results. All simulations were run in parallel using the DelftBlue supercomputer (Delft High Performance Computing Centre DHPC).

Disclosure statement

No potential conflict of interest was reported by the author(s).

Funding

The project is funded by the Netherlands Enterprise Agency (RVO: Rijksdienst voor Ondernemend Nederland) [grant number MOB21012].

ORCID

Konstantinos Zoumpourlos http://orcid.org/0000-0003-1046-5613
Rinze Geertsma http://orcid.org/0000-0001-5125-0358
Robert van de Ketterij http://orcid.org/0000-0003-1774-3997
Andrea Coraddu http://orcid.org/0000-0001-8891-4963

References

Abraham J. 1997. What is adequate resolution in the numerical computations of transient jets? SAE Technical Paper. 970051:141–155.

Agarwal AK, Gautam A, Sharma N, Singh AP. 2019. Methanol and the alternate fuel economy. Springer.
Agarwal AK, Kumar V, Ankur Kalwar AJ. 2022. Fuel injection strategy optimisation and experimental performance and emissions evaluation of diesel displacement by port fuel injected methanol in a retrofitted mid-size genset engine prototype. Energy. 248:123593.
Ait Allal A, Mansouri K, Youssfi M, Qbadou M. 2019. Toward an evaluation of marine fuels for a clean and efficient autonomous ship propulsion energy. Mater Today Proc. 13:486–495.
American Bureau of Shipping (ABS). 2020. Pathways to sustainable shipping. Report No:. [accessed 2022 Jul 7]. https://www.hernieuwbarebrandstoffen.nl/post/pathways-to-sustainable-shipping.
Amsden AA, O'Rourke PJ, Butler TD. 1989. Kiva-ii: a computer program for chemically reactive flows with sprays. Los Alamos (NM): Los Alamos National Lab. (LANL). Report No.
Badawy T, Xu H, Li Y. 2022. Macroscopic spray characteristics of iso-octane, ethanol, gasoline and methanol from a multi-hole injector under flash boiling conditions. Fuel. 307:121820.
Baumgarten C. 2006. Mixture formation in internal combustion engines. Springer Science & Business Media.
Beale JC, Reitz RD. 1999. Modeling spray atomization with the kelvin-helmholtz/rayleigh-taylor hybrid model. Atomization Sprays. 9(6):623–650.
BETA. BETA CAE systems website. [accessed 2023 Nov 13]. https://www.beta-cae.com/.
Bosklopper J, Sapra H, van de Ketterij R, van Sluijs W, Bekdemir C, de Vos P, Visser K. 2020. Experimental study on a retrofitted marine size spark-ignition engine running on port-injected 100% methanol. In: Conference proceedings of INEC (Vol. 2020).
Cabezas K. M., Liu X., Im H. G. 2022. Characteristics of methanol and iso-octane under flashing and non-flashing conditions in ecn-g spray (No. 2022-01-0496). SAE Technical Paper.
CMT – Clean Mobility & Thermofluids website. Virtual injection rate generator. [accessed 2023 Sep 5]. https://www.cmt.upv.es/#/ecn/download/InjectionRateGenerator/InjectionRateGenerator/.
Convergent Science. CONVERGE CFD software website. [accessed 2023 Nov 13]. https://convergecfd.com/.
Convergent Science Inc. 2022. Converge Manual v3.0.
Curran S, Onorati A, Payri R, Agarwal AK, Arcoumanis C, Bae C, Boulouchos K, et al. 2024. The future of ship engines: renewable fuels and enabling technologies for decarbonization. Int J Engine Res. 25(1):85–110.
Delft High Performance Computing Centre (DHPC). 2022. DelftBlue Supercomputer (Phase 1). https://www.tudelft.nl/dhpc/ark/delftbluephase1.
Dierickx J, Sileghem L, Verhelst S. 2019. Efficiency and emissions of a high-speed marine diesel engine converted to dual-fuel operation with methanol. In CIMAC world congress on combustion engine (pp. 1–14). Cimac.
Dierickx J, Verbiest J, Janvier T, Peeters J, Sileghem L, Verhelst S. 2021. Retrofitting a high-speed marine engine to dual-fuel methanol-diesel operation: a comparison of multiple and single point methanol port injection. Fuel Commun. 7:100010.
Duronio F, De Vita A, Allocca L, Anatone M. 2020. Gasoline direct injection engines–a review of latest technologies and trends. Part 1: Spray breakup process. Fuel. 265:116948.
ECN. Engine combustion network. [accessed 2023 Sep 1]. https://ecn.sandia.gov/.
Ferziger JH, Perić M, Street RL. 2002. Computational methods for fluid dynamics. Vol. Springer.
Ghosh A, Boggavarapu P, Ravikrishna RV. 2020. Measurement of liquid and vapor penetration of evaporating methanol sprays. Atomization Sprays. 30(10):741–757.
Ghosh A, Ravikrishna RV. 2021. Evaporating spray characteristics of methanol-in-diesel emulsions. Fuel. 290:119730.
Gong Y, Liu S, Li Y. 2007. Investigation on methanol spray characteristics. Energy Fuels. 21(5):2991–2997.
Han Z, Reitz RD. 1995. Turbulence modeling of internal combustion engines using rng κ-ε models. Combust Sci Technol. 106(4–6):267–295.
Horvath A. 1974. Redlich-kwong equation of state: review for chemical engineering calculations. Chem Eng Sci. 29(5):1334–1340.
Hsiang LP, Faeth GM. 1995. Drop deformation and breakup due to shock wave and steady disturbances. Int J Multiphase Flow. 21(4):545–560.
Hwang J, Weiss L, Karathanassis IK, Koukouvinis P, Pickett LM, Skeen SA. 2020. Spatio-temporal identification of plume dynamics by 3d computed tomography using engine combustion network spray g injector and various fuels. Fuel. 280:118359.
International Maritime Organization. 2020. International maritime organization: fourth greenhouse gas study 2020. Report No:. [accessed 2023 Feb 5]. https://www.imo.org/en/OurWork/Environment/Pages/Fourth-IMO-Greenhouse-Gas-Study-2020.aspx.
Issa RI. 1986. Solution of the implicitly discretised fluid flow equations by operator-splitting. J Comput Phys. 62(1):40–65.
Kessel DG. 2000. Global warming–facts, assessment, countermeasures. J Pet Sci Eng. 26(1–4):157–168.
Korberg AD, Brynolf S, Grahn M, Skov IR. 2021. Techno-economic assessment of advanced fuels and propulsion systems in future fossil-free ships. Renewable Sustainable Energy Rev. 142:110861.
Kundu PK, Cohen IM, Dowling DR. 2015. Fluid mechanics. Academic Press.
Kurien C, Mittal M. 2022. Review on the production and utilization of green ammonia as an alternate fuel in dual-fuel compression ignition engines. Energy Convers Manage. 251:114990.
Li H, Beji T, Verhelst S. 2021. Improving the calculation of evaporating sprays for medium-speed marine-engine-like conditions. Atomization Sprays. 31(8):55–79.
Lichtarowicz A, Duggins RK, Markland E. 1965. Discharge coefficients for incompressible non-cavitating flow through long orifices. J Mech Eng Sci. 7(2):210–219.
Liu AB, Mather D, Reitz RD. 1993. Modeling the effects of drop drag and breakup on fuel sprays. SAE Trans. 930072:83–95.
Liu K, Chen C, Su M, Zhou W, Wang Q, Oppong F, Li L, Xu C. 2022. Experimental study of the macroscopic characteristics of methanol low-pressure injection spray. Int J Energy Res. 46(15):23259–23272.
Maes N, Dam N, Somers B, Lucchini T, D'Errico G, Hardy G. 2016. Experimental and numerical analyses of liquid and spray penetration under heavy-duty diesel engine conditions. SAE Int J Fuels Lubr. 9(1):108–124.
Maes N, Skeen SA, Bardi M, Fitzgerald RP, Malbec LM, Bruneaux G, Pickett LM, Yasutomi K, Martin G. 2020. Spray penetration, combustion, and soot formation characteristics of the ecn spray c and spray d injectors in multiple combustion facilities. Appl Therm Eng. 172:115136.
MAN Energy Solutions. MAN B&W ME-LGIM two-stroke dual-fuel engine. [accessed 2023 Oct 18]. https://www.man-es.com/marine/products/two-stroke-engines/man-b-w-me-lgim.
Matamis A, Lonn S, Tuner M, Andersson O, Richter M. 2020. Optical characterization of methanol sprays and mixture formation in a compression-ignition heavy-duty engine (No. 2020-01-2109). SAE Technical Paper.
McKinlay CJ, Turnock SR, Hudson DA. 2021. Route to zero emission shipping: hydrogen, ammonia or methanol? Int J Hydrogen Energy. 46(55):28282–28297.
Miller R, Harstad K, Bellan J. 1998. Evaluation of equilibrium and non-equilibrium evaporation models for many-droplet gas-liquid flow simulations. Int J Multiphase Flow. 24(6):1025–1055.
Nemati A, Ong JC, Walther JH. 2022. CFD analysis of combustion and emission formation using urans and les under large two-stroke marine engine-like conditions. Appl Therm Eng. 216:119037.
O'Rourke PJ. 1989. Statistical properties and numerical implementation of a model for droplet dispersion in a turbulent gas. J Comput Phys. 83(2):345–360.
O'Rourke PJ, Amsden AA. 1987. The tab method for numerical calculation of spray droplet breakup. SAE Technical Paper. Report No.
Panda K, Ramesh A. 2022. HCCI combustion of methanol along with diesel through novel injection strategies and its potential over conventional dual fuel combustion. Fuel. 324:124766.
Paredi D, Lucchini T, D'Errico G, Onorati A, Pickett L, Lacey J. 2020. Validation of a comprehensive computational fluid dynamics methodology to predict the direct injection process of gasoline sprays using spray g experimental data. Int J Engine Res. 21(1):199–216.
Payri R, García J, Salvador F, Gimeno J. 2005. Using spray momentum flux measurements to understand the influence of diesel nozzle geometry on spray characteristics. Fuel. 84(5):551–561.
Payri R, Gimeno J, Cuisano J, Arco J. 2016. Hydraulic characterization of diesel engine single-hole injectors. Fuel. 180:357–366.
Pickett LM, Manin J, Payri R, Bardi M, Gimeno J. 2013. Transient rate of injection effects on spray development. SAE Technical Paper. Report No.
Pipicelli M, Di Luca G, Ianniello R, Gimelli A, Beatrice C. 2022. Alcohol fuels in compression ignition engines. In: Energy, environment, and sustainability. Springer Nature; p. 9–31.
Pope S. 1978. An explanation of the turbulent round-jet/plane-jet anomaly. AIAA J. 16(3):279–281.
Portin K. 2015. Wärtsilä gas engine development and methanol adaptation: Classnk seminar. Report No:. [accessed 2023 Oct 18]. https://www.classnk.or.jp/classnk-rd/assets/pdf/V_Wartsila_Gas_Engine_Development_Methanol_Adaptation.pdf.
Post SL, Abraham J. 2002. Modeling the outcome of drop–drop collisions in diesel sprays. Int J Multiphase Flow. 28(6):997–1019.
Reitz RD. 1986. Mechanism of breakup of round liquid jets. Encycl Fluid Mech. 10.
Reitz RD, Diwakar R. 1987. Structure of high-pressure fuel sprays. SAE Technical Paper. 870598:492–509.
Reitz RD, Ogawa H, Payri R, Fansler T, Kokjohn S, Moriyoshi Y, Agarwal A, Arcoumanis D, Assanis D, Bae C, et al. 2020. IJER editorial: the future of the internal combustion engine. Int J Engine Res. 21(1):3–10.

Saha K, Quan S, Battistoni M, Som S, Senecal P, Pomraning E. 2017. Coupled eulerian internal nozzle flow and Lagrangian spray simulations for GDI systems. SAE Technical Paper. Report No.

Schmidt DP, Rutland CJ. 2000. A new droplet collision algorithm. J Comput Phys. 164(1):62–80.

Senecal P, Pomraning E, Richards K, Som S. 2012. Grid-convergent spray models for internal combustion engine CFD simulations. In: Internal combustion engine division fall technical conference. Vol. 55096. American Society of Mechanical Engineers; p. 697–710.

Senecal P, Richards K, Pomraning E, Yang T, Dai M, McDavid R, Patterson M, Hou S, Shethaji T. 2007. A new parallel cut-cell cartesian CFD code for rapid grid generation applied to in-cylinder diesel engine simulations. SAE Technical Paper. Report No.

Singh J, Dhar A, Kumar P. 2022. Methanol fuel in compression ignition engines. In: Energy, environment, and sustainability. Springer Nature; p. 71–101.

Soni DK, Gupta R. 2016. Optimization of methanol powered diesel engine: a CFD approach. Appl Therm Eng. 106:390–398.

Sphicas P, Pickett LM, Skeen S, Frank J, Lucchini T, Sinoir D, D'Errico G, Saha K, Som S. 2017. A comparison of experimental and modeled velocity in gasoline direct-injection sprays with plume interaction and collapse. SAE Int J Fuels Lubr. 10(1):184–201.

Spray G E. Engine combustion network Spray-G conditions. [accessed 2023 Oct 7]. https://ecn.sandia.gov/gasoline-spray-combustion/target-condition/spray-g-operating-condition/.

Spray M E. Engine combustion network Spray-M data. [accessed 2023 Oct 7]. https://ecn.sandia.gov/data/sandia-spray-m-data/.

Subramaniam S. 2013. Lagrangian–Eulerian methods for multiphase flows. Prog Energy Combust Sci. 39(2–3):215–245.

Verhelst S, Turner JW, Sileghem L, Vancoillie J. 2019. Methanol as a fuel for internal combustion engines. Prog Energy Combust Sci. 70:43–88.

Wang X, Gao J, Jiang D, Huang Z, Chen W. 2005. Spray characteristics of high-pressure swirl injector fueled with methanol and ethanol. Energy Fuels. 19(6):2394–2401.

Wang Y, Dong P, Long W, Tian J, Wei F, Wang Q, Cui Z, Li B. 2022. Characteristics of evaporating spray for direct injection methanol engine: comparison between methanol and diesel spray. Processes. 10(6):1132.

Wouters C, Burkardt P, Steeger F, Fleischmann M, Pischinger S. 2023. Comprehensive assessment of methanol as an alternative fuel for spark-ignition engines. Fuel. 340:127627.

Zembi J, Battistoni M, Pandal A, Mounaïm-Rousselle C, Pelé R, Brequigny P, Hespel C. 2023. Numerical study of ammonia spray with a GDI engine injector. J Ammonia Energy. 1(1):59–73.

Zeng W, Xu M, Zhang G, Zhang Y, Cleary DJ. 2012a. Atomization and vaporization for flash-boiling multi-hole sprays with alcohol fuels. Fuel. 95:287–297.

Zeng W, Xu M, Zhang M, Zhang Y, Cleary D. 2010. Characterization of methanol and ethanol sprays from different DI injectors by using mie-scattering and laser induced fluorescence at potential engine cold-start conditions. SAE Technical Papers.

Zeng W, Xu M, Zhang M, Zhang Y, Cleary DJ. 2012b. Macroscopic characteristics for direct-injection multi-hole sprays using dimensionless analysis. Exp Therm Fluid Sci. 40:81–92.

Zhu Z, Gu H, Zhu Z, Wei Y, Zeng K, Liu S. 2021. Investigation on mixture formation and combustion characteristics of a heavy-duty SI methanol engine. Appl Therm Eng. 196:117258.

Zincir B, Deniz C. 2021. Methanol as a fuel for marine diesel engines. In: Energy, environment, and sustainability. Springer Nature; p. 45–85.

Zoumpourlos K, Coraddu A, Geertsma R, van de Ketterij R. 2023. Evaluation of methanol sprays in marine internal combustion engines: a case study for port fuel injection systems. Modell Optim Ship Energy Syst. 2023. https://proceedings.open.tudelft.nl/moses2023/article/view/655.